Scanning Electrochemistry Microscopy (SECM) in the Study of Electron Transfer Kinetics at Liquid/Liquid Interfaces: Beyond the Constant Composition Approximation

Anna L. Barker and Patrick R. Unwin*,†

Department of Chemistry, University of Warwick, Coventry CV4 7AL, U.K.

Shigeru Amemiya, Jungfen Zhou, and Allen J. Bard*,‡

Department of Chemistry and Biochemistry, University of Texas at Austin, Austin, Texas 78712

Received: April 29, 1999; In Final Form: June 19, 1999

A numerical model is developed for the SECM feedback mode for the case of irreversible electron transfer (ET) processes at the interface between two immiscible electrolyte solutions (ITIES). In this application, a redox-active species is electrogenerated by the reduction/oxidation of the oxidized/reduced form of a couple at an ultramicroelectrode (UME) tip located in one liquid (phase 1). The tip is positioned close to the interface with a second immiscible liquid (phase 2), that contains the oxidized/reduced half of another redox couple. If ET occurs between the tip-generated species in phase 1 and the redox-active species in phase 2, then the original species in phase 1 is regenerated at the interface and undergoes positive feedback at the tip, enhancing the steady-state current. The feedback current, for a given separation between the tip and the interface, is shown to depend on the ratio of the concentrations of the redox-active species in the two phases, their relative diffusion coefficients, and the rate constant for the redox reaction. The results of the model are used to identify the conditions under which (i) diffusion in phase 2 has to be considered and; (ii) a simpler limiting (constant composition) model for phase 2, employed to analyze earlier SECM experiments, can be used. In addition to diversifying the range of conditions under which redox reactions at ITIES can be studied, the results of the model demonstrate that there are considerable advantages to lifting the constant composition restriction on phase 2 for the accurate characterization of rapid redox reactions. The theoretical predictions are examined through experimental studies of electron transfer between the electrogenerated, oxidized form of zinc-21H, 23H-tetraphenylporphine (ZnPor) in benzene or benzonitrile and the reductants $Fe(CN)_6^{4-}$, $Ru(CN)_6^{4-}$, $Mo(CN)_8^{4-}$, or $FeEDTA^{2-}$ (where EDTA denotes ethylenediaminetetraacetic acid) in an aqueous solution. Bimolecular rate constants for each of these systems are reported, with the potential across the ITIES biased with either perchlorate or tetrafluoroborate ions in each phase.

Introduction

Scanning electrochemical microscopy (SECM) has emerged as a powerful approach for studying the kinetics of electron,[1−7] ion[8−11] and molecular[10,12] transfer across an ITIES. Studies of ET have employed the feedback mode,[13] in which a redox-active species, e.g., Ox_1 is electrogenerated from a reduced form, Red_1, at an UME tip located in one liquid (phase 1), close to the interface with a second immiscible liquid (phase 2) that contains the reduced form of a separate redox couple (Red_2). As shown schematically in Figure 1, if a redox reaction occurs between Ox_1 and Red_2

$$Ox_1 + Red_2 \rightarrow Ox_2 + Red_1$$

then Red_1 is regenerated at the interface and diffuses back to the tip. The effect of this positive feedback of Red_1 is to enhance the current compared to the situation where there is no redox reaction and Red_1 simply reaches the tip by hindered diffusion.

There are four main processes that contribute to the magnitude of the tip current:[1] (i) mediator diffusion in phase 1 between the tip and the ITIES, (ii) mediator diffusion in phase 2, (iii) the rate of the reaction at the ITIES, and (iv) ion transport across the ITIES to balance charge. The kinetics of the interfacial reaction can be evaluated from the tip current response, provided the contributions from the other processes are either known or nonlimiting.

The advantages of studying interfacial redox reactions at an ITIES by SECM feedback are now well established.[1,4] In particular, (i) the SECM current allows discrimination between electron and ion transfer processes at the interface; (ii) distortions associated with *iR* drop and charging current are eliminated; (iii) it is not necessary to externally bias the interface, thereby avoiding complications due to the polarization window of the ITIES and the variation of the interfacial properties with applied potential. In addition, it is generally proven that SECM allows the study of rapid interfacial processes, since the micrometer and submicrometer dimensions of both the UME and the tip/interface gap promote high rates of mass transport.

Previous SECM liquid/liquid feedback experiments often employed a high concentration of reactant in phase 2 compared to that of the mediator in phase 1 to avoid the complication of diffusional effects in the second phase.[1,4,7] While this approach simplifies the model, it does limit the use of lower concentrations

† E-mail: p.r.unwin@warwick.ac.uk.
‡ E-mail: ajbard@mail.utexas.edu.

10.1021/jp991414l CCC: $18.00
Published on Web 08/04/1999

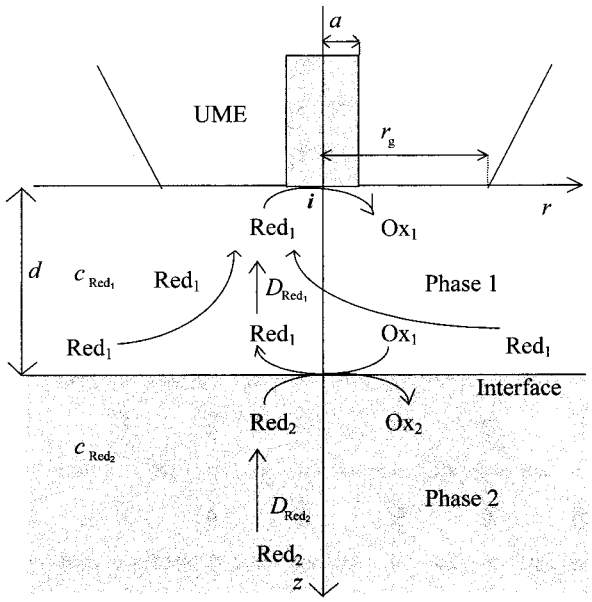

Figure 1. Schematic of SECM feedback at an ITIES with the coordinate system used for the theoretical model. The coordinates r and z are measured from the center of the UME in the radial and normal directions, respectively. The UME is characterized by an electrode radius, a, and r_g is the distance from the center of the electrode to the edge of the surrounding insulating glass sheath. The ITIES is located at distance, d. Species Red_1 and Ox_1 are confined to phase 1, while species Red_2 and Ox_2 are present in phase 2.

in the second phase. Moreover, as shown in this paper, the use of lower concentrations is particularly beneficial in determining the rate constant when the electron transfer reaction is rapid. Because of the advantages of SECM, compared to alternative methods, we develop here a more general theory to both considerably extend the applicability and to identify precisely when the constant composition assumption is valid. We have recently reported a theoretical model which includes depletion and diffusion effects in the second phase for the process of SECM induced transfer (SECMIT),[10] and this paper serves to extend the theory developed therein to the SECM feedback mode.

A theoretical model is developed for the case of an irreversible, driven ET process at the interface, i.e. the situation where the potentials of the redox couples in the two phases are widely separated. The model would require only simple modifications to be applicable to the cases of reversible and quasireversible ET. Because of the number of parameters involved in the problem, the aim of this paper is to give a general guide to the conditions where depletion effects in the second phase become important and to state the implications for the analysis of ET kinetics. The predictions from the model are examined through experimental studies of ET between electrogenerated $ZnPor^{+\bullet}$ in benzene or benzonitrile and the reductants $Fe(CN)_6^{4-}$, $Ru(CN)_6^{4-}$, $Mo(CN)_8^{4-}$, or $FeEDTA^{2-}$ in an aqueous solution. These studies clearly demonstrate that lifting the constant composition restriction on the second phase is particularly advantageous for the accurate measurement of rapid redox reactions.

Theory

Formulation of the Problem. Consider the case where the diffusion coefficients of Red_1 and Ox_1 are equal, i.e., $D_{Red_1} = D_{Ox_1}$, with only the reactant, Red_1, initially present in phase 1 at concentration $c^*_{Red_1}$. This is a useful assumption, since it allows the principle of mass conservation to be invoked in phase 1:

$$0 \le r \le r_g,\ 0 < z < d:\ c_{Ox_1}(r,z) = c^*_{Red_1} - c_{Red_1}(r,z) \qquad (2)$$

where $c_{Ox_1}(r,z)$ and $c_{Red_1}(r,z)$ are the spatial-dependent concentrations of Ox_1 and Red_1, respectively, within the region of interest (see Figure 1), defined in terms of r and z, which are the coordinates in the directions radial and normal to the electrode surface measured from the center of the electrode. The parameters d and r_g, respectively, denote the location of the liquid/liquid interface and the edge of the glass sheath surrounding the UME. The use of eq 2 simplifies the problem to the consideration of species Red_1 and Red_2 alone. Although the diffusion coefficients of Red_1 and Ox_1 may differ slightly in real systems, it has been shown that under steady-state conditions (of interest in this paper), the ratio D_{Ox_1}/D_{Red_1} has no effect on the positive feedback current characteristics.[14]

Time-dependent diffusion equations, appropriate to the axisymmetric SECM geometry, can be written for the species of interest in each phase

$$\text{Phase 1:}\ \frac{\partial c_{Red_1}}{\partial t} = D_{Red_1}\left[\frac{\partial^2 c_{Red_1}}{\partial r^2} + \frac{1}{r}\frac{\partial c_{Red_1}}{\partial r} + \frac{\partial^2 c_{Red_1}}{\partial z^2}\right] \qquad (3)$$

$$\text{Phase 2:}\ \frac{\partial c_{Red_2}}{\partial t} = D_{Red_2}\left[\frac{\partial^2 c_{Red_2}}{\partial r^2} + \frac{1}{r}\frac{\partial c_{Red_2}}{\partial r} + \frac{\partial^2 c_{Red_2}}{\partial z^2}\right] \qquad (4)$$

where c_{Red_2} and D_{Red_2} are, respectively, the concentration and diffusion coefficient of species Red_2 in phase 2, and t is time.

In order to calculate the tip current response, the diffusion equations must be solved subject to the boundary and initial conditions of the system. Prior to the potential step, phase 1 and 2 contain only species Red_1 and Red_2, respectively. The initial condition is thus

$$t = 0;\ \ 0 \le r \le r_g,\ \ 0 \le z \le d:\ \ c_{Red_1} = c^*_{Red_1}$$
$$0 \le r \le r_g,\ \ z > d:\ \ c_{Red_2} = c^*_{Red_2} \qquad (5)$$

where $c^*_{Red_2}$ denotes the initial bulk concentration of Red_2 in phase 2.

The potential of the UME tip is stepped from a value where no electrode reaction occurs, to one sufficient to drive the oxidation of Red_1 at a diffusion-controlled rate. Species Red_1 is assumed to be inert with respect to the insulating glass sheath surrounding the electrode and to remain at bulk concentration values beyond the radial edge of the tip (throughout phase 1). In phase 2, species Red_2 attains its bulk concentration for $r > r_g$ and at a semi-infinite distance from the electrode. Consequently, the exterior boundary conditions may be summarized as follows:

$$z = 0,\ \ 0 \le r \le a:\ \ c_{Red_1} = 0 \qquad (6)$$

$$z = 0,\ \ a < r \le r_g:\ \ D_{Red_1}\frac{\partial c_{Red_1}}{\partial z} = 0 \qquad (7)$$

$$z \to \infty,\ \ 0 \le r \le r_g:\ \ c_{Red_2} = c^*_{Red_2} \qquad (8)$$

$$r > r_g,\ \ 0 < z < d:\ \ c_{Red_1} = c^*_{Red_1}$$
$$z > d:\ \ c_{Red_2} = c^*_{Red_2} \qquad (9)$$

This latter condition is valid provided that $RG = r_g/a \geq 10$,[15] where a is the radius of the electrode.

The axisymmetric cylindrical geometry of the SECM implies

$$r = 0,\ 0 < z < d:\ D_{\mathrm{Red}_1}\frac{\partial c_{\mathrm{Red}_1}}{\partial r} = 0$$
$$z > d:\ D_{\mathrm{Red}_2}\frac{\partial c_{\mathrm{Red}_2}}{\partial r} = 0 \qquad (10)$$

The final internal boundary condition applies to the interface and relates the flux of species Red_1 and Red_2, at the ITIES, to the rate of the second-order redox reaction occurring at the interface.

$z = d$, all r:

$$D_{\mathrm{Red}_1}\frac{\partial c_{\mathrm{Red}_1}}{\partial z} = D_{\mathrm{Red}_2}\frac{\partial c_{\mathrm{Red}_2}}{\partial z} = k_{12}(c^*_{\mathrm{Red}_1} - c_{\mathrm{Red}_1})c_{\mathrm{Red}_2} \qquad (11)$$

where k_{12} is the heterogeneous bimolecular rate constant (cm s^{-1} M^{-1}).

To formulate a general solution, the following dimensionless terms are introduced:

$$\tau = \frac{tD_{\mathrm{Red}_1}}{a^2} \qquad (12)$$

$$R = \frac{r}{a} \qquad (13)$$

$$Z = \frac{z}{a} \qquad (14)$$

$$\gamma = \frac{D_{\mathrm{Red}_2}}{D_{\mathrm{Red}_1}} \qquad (15)$$

$$C_{\mathrm{Red}_i} = \frac{c_{\mathrm{Red}_i}}{c^*_{\mathrm{Red}_i}} \text{ where } i \text{ denotes either 1 or 2.} \qquad (16)$$

$$K = \frac{k_{12}ac^*_{\mathrm{Red}_2}}{D_{\mathrm{Red}_1}} \qquad (17)$$

$$K_r = \frac{c^*_{\mathrm{Red}_2}}{c^*_{\mathrm{Red}_1}} \qquad (18)$$

It should be clear how these terms affect the diffusion equations (eqs 3 and 4) and associated boundary and initial conditions.

The tip current response is calculated as a function of time and tip/interface separation, for particular K_r, K, and γ values. The UME current is related to the flux of Red_1 at the electrode surface and hence the dimensionless current ratio is given by[16]

$$\frac{i}{i(\infty)} = \frac{\pi}{2}\int_0^1 \left(\frac{\partial C_{\mathrm{Red}_1}}{\partial Z}\right)_{Z=0} RdR \qquad (19)$$

where $i(\infty)$ is the steady-state diffusion-limited current at an inlaid disk electrode positioned at an effectively infinite distance from the interface.[17]

$$i(\infty) = 4nFaD_{\mathrm{Red}_1}c^*_{\mathrm{Red}_1} \qquad (20)$$

Method of Solution. Numerical solutions were achieved using the alternating direction implicit finite-difference method (ADIFDM).[18] The application of this method to a variety of SECM problems has been described elsewhere.[10,12,14,16,19] The following brief account of the modifications required to treat the internal boundary condition in the above model should be read with reference to more detailed descriptions of the ADIFDM as applied to SECM.[10,16,19]

The ADIFDM involves the construction of implicit finite difference equations at successive half-time intervals, respectively, for the R and Z directions. The finite-difference grid employed was as used previously for two-phase problems.[10] For the first half-time step, in which concentrations were calculated in the radial direction from known values deduced in the previous half-time step, the calculation proceeded from the points $j = 1$ to $j = \mathrm{NE} + \mathrm{NG} - 1$, where j denotes the grid points in the radial direction running from $j = 0$ at $R = 0$ to $j = \mathrm{NE}$ at $R = 1$ (over the tip electrode) and $j = \mathrm{NE} + 1$ to $j = \mathrm{NE} + \mathrm{NG}$ over the insulating glass sheath. This results in $\mathrm{NE} + \mathrm{NG} - 1$ simultaneous equations and $\mathrm{NE} + \mathrm{NG} - 1$ unknowns for each grid point, k, in the Z coordinate. After application of the boundary conditions above, these equations may be expressed as a tridiagonal matrix, the solution of which is found using the Thomas algorithm.[20]

The calculation was performed for each point on the finite-difference grid, over phase 1 (from $k = 1$ to $k = \mathrm{NZ1} - 1$) and then phase 2 (from $k = \mathrm{NZ1} + 1$ to $k = \mathrm{NZ1} + \mathrm{NZ2} - 1$). The electrode was at $k = 0$, the ITIES was located at $k = \mathrm{NZ1}$, and $k = \mathrm{NZ1} + \mathrm{NZ2}$ corresponded to a sufficient distance from the UME for a semi-infinite boundary condition to be applicable (see ref 10). At the end of each first half-time step, the interior boundary condition (eq 11), in finite-difference form, was used to update the concentrations of species Red_1 and Red_2 at the interface. Those remaining exterior boundary concentrations involving no-flux boundary conditions were also updated.

During the second half-time step, concentrations in the Z direction were calculated from the values of the concentrations in the radial direction, evaluated in the first half-time step. For $k = 1$ to $\mathrm{NZ1} - 1$ and $k = \mathrm{NZ1} + 1$ to $\mathrm{NZ1} + \mathrm{NZ2} - 1$, the approach was similar to that employed previously.[10] However, for $k = \mathrm{NZ1}$ the finite-difference equations derived from the interior boundary condition are

$$^{\mathrm{Red}_1}C^{**}_{j,\mathrm{NZ1}-1} - {}^{\mathrm{Red}_1}C^{**}_{j,\mathrm{NZ1}}(1 + K\Delta Z^{\mathrm{Red}_2}C^{**}_{j,\mathrm{NZ1}}) + K\Delta Z^{\mathrm{Red}_2}C^{**}_{j,\mathrm{NZ1}} = 0 \qquad (21)$$

$$^{\mathrm{Red}_1}C^{**}_{j,\mathrm{NZ1}}\left(\frac{K\Delta Z_{\mathrm{Red}_2}C^{**}_{j,\mathrm{NZ1}}}{K_r\gamma}\right) - {}^{\mathrm{Red}_2}C^{**}_{j,\mathrm{NZ1}}\left(1 + \frac{K\Delta Z}{K_r\gamma}\right) + {}^{\mathrm{Red}_2}C^{**}_{j,\mathrm{NZ1}+1} = 0 \qquad (22)$$

In eqs 21 and 22, $^{\mathrm{Red}_i}C^{**}_{j,\mathrm{NZ1}+m}$ is the new (normalized) concentration of Red_i (where i is either 1 or 2) at the loci j, $\mathrm{NZ1} + m$ (where m is -1, 0 or $+1$). ΔZ is the grid spacing in the Z direction (which is uniform in phase 1, expanding with increasing distance in phase 2, and matched at the interface, as described in ref 10). It is apparent from these equations that the calculation of $^{\mathrm{Red}_i}C^{**}_{j,k}$ for $k = 1$ to $k = \mathrm{NZ1} + \mathrm{NZ2}$, for each value of j, requires a prior knowledge of $^{\mathrm{Red}_2}C^{**}_{j,\mathrm{NZ1}}$ for the matrix equations to reduce to tridiagonal form. This problem was overcome by adopting an iterative procedure in which, for a particular value of j, $^{\mathrm{Red}_2}C^{**}_{j,\mathrm{NZ1}}$ was initially approximated by $^{\mathrm{Red}_2}C^{*}_{j,\mathrm{NZ1}}$ (calculated in the first-half time step). Following the calculation of $^{\mathrm{Red}_i}C^{**}_{j,k}$ (for $i = 1$ and 2), the procedure was

repeated using the newly determined value for $^{Red_2}C^{**}_{j,NZ1}$ until values of $^{Red_2}C^{**}_{j,NZ1}$ were unchanged (precision 10^{-10}) upon further iteration. At the end of each second half-time step all matrix elements were checked to verify convergence within the required precision (10^{-8}).

Theoretical Results and Discussion

The numerical model developed above involves the parameters K, γ, K_r, and the normalized tip/interface distance, $L = d/a$. The aim of this section is to analyze the effect of these parameters on the tip current. Although the ADIFDM calculates the chronoamperometric response of the UME probe, the results described here are for the steady-state characteristics, determined from the long-time limit, which are of primary interest in SECM feedback experiments on liquid/liquid interfaces.[1-7] The simulations reported in this section were performed for an UME characterized by $RG = r_g/a = 10$, which is a typical value used in SECM experiments and theoretical treatments.

The effect on the normalized approach curves of allowing K_r to take finite values is illustrated in Figure 2, which shows simulated data for three rate constants for redox couples characterized by $\gamma = 1$. The rate parameters considered are typical of the upper, medium, and lower constants that might be encountered in feedback measurements at liquid/liquid interfaces. In each case, values of $K_r = 1000$ or 100 yield approach curves which are identical to the earlier solution for no depletion in phase 2.[1,19b] This behavior was predicted earlier[1] and is expected, given the relatively high concentration of Red_2 compared to Red_1. This ensures that the concentration of Red_2 adjacent to the liquid/liquid interface is maintained close to the bulk solution value, even when the redox process, eq 1, is driven at a fast rate [Figure 2(i)].

For $K_r \leq 10$, the calculated normalized currents are lower than predicted by the constant composition model, particularly at close tip/interface separations, where the diffusion rate of the Red_1/Ox_1 couple in phase 1 is highest and competes effectively with the diffusion of Red_2 in phase 2. As expected, the deviation of the current from that predicted, assuming constant composition conditions, becomes increasingly significant as K_r is reduced, resulting in increasing diffusional limitations from Red_2 in phase 2. On the basis of the data in Figure 2, the constant composition assumption is seen to break down for $K_r \leq 10$, irrespective of the size of the rate constant characterizing the interfacial process. The conditions under which the approximation becomes invalid are discussed further below.

The reasons for the deviation of the full model from the constant composition model are apparent when the concentrations of Red_1 and Red_2 are examined. Because of the axisymmetric SECM geometry, the concentration profiles of Red_1 and Red_2 are shown as cross-sections over the domain $R \geq 0$, $Z \geq 0$, as illustrated schematically in Figure 3. Note that in this figure the tip position has been inverted compared to that in Figure 1. Figures 4, 5 and 6 show profiles for $K = 100$, 10, and 1, respectively, at a normalized tip/interface separation, $d/a = 0.1$ (which is typical of the smallest d/a attainable in SECM measurements). In each case, normalized concentration distributions are shown in terms of C_{Red_i} ($i = 1$ or 2) for $K_r = 1000$, 10, and 5. With the former value of K_r, phase 2 is maintained at constant composition for the range of rate constants considered, and profiles for this case are thus provided for phase 1 only. These latter profiles show the expected changes in the concentration of Red_1 as the kinetics change from the fast limit, where positive feedback is observed [Figure 4(i)], to a situation where the turnover of Red_1 at the interface becomes increasingly slow, so that hindered diffusion (negative feedback) becomes important [Figures 5(i) and 6(i)].

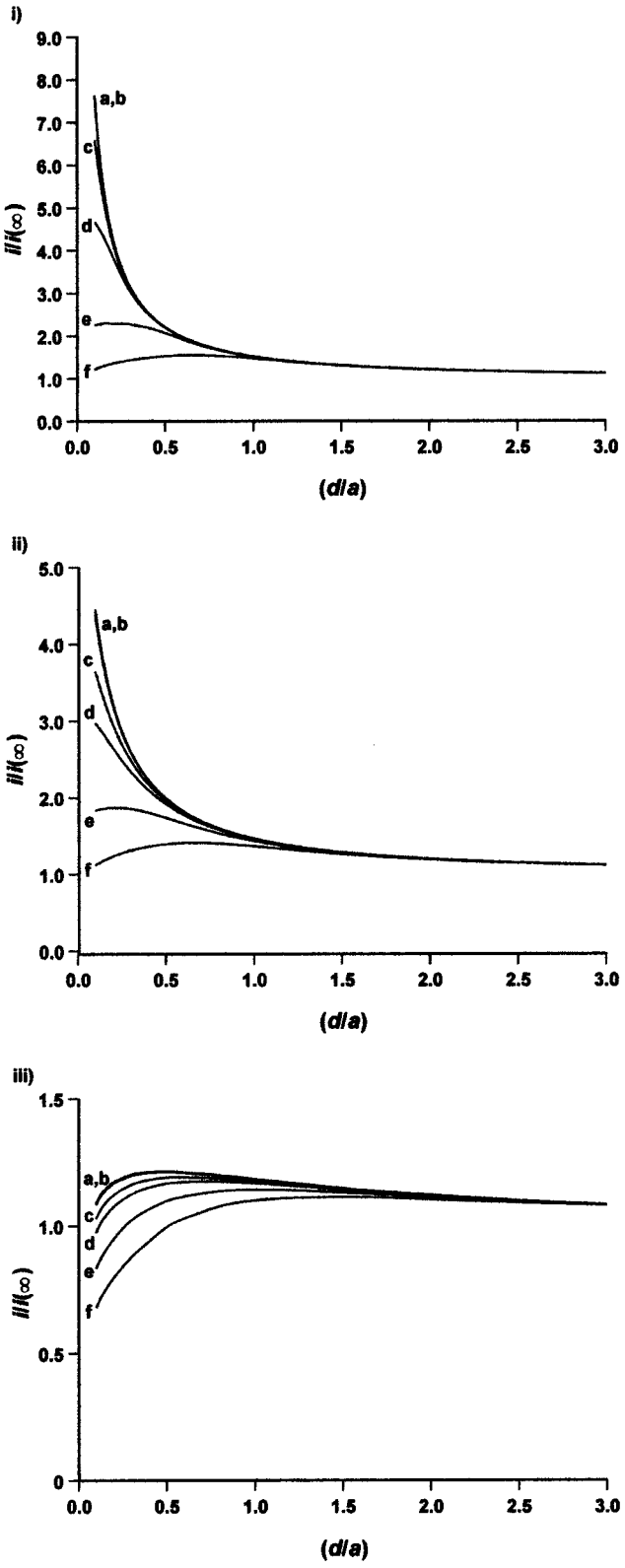

Figure 2. Simulated normalized steady-state current as a function of tip/interface distance for (i) $K = 100$, (ii) $K = 10$, and (iii) $K = 1$. In each case $\gamma = 1$ and K_r takes the values (a) 1000, (b) 100, (c) 10, (d) 5, (e) 2, and (f) 1.

In the fast kinetic regime ($K = 100$), the turnover of Red_1 at the portion of the interface directly under the tip is sufficiently fast that Red_2 is depleted in this interfacial region, even when

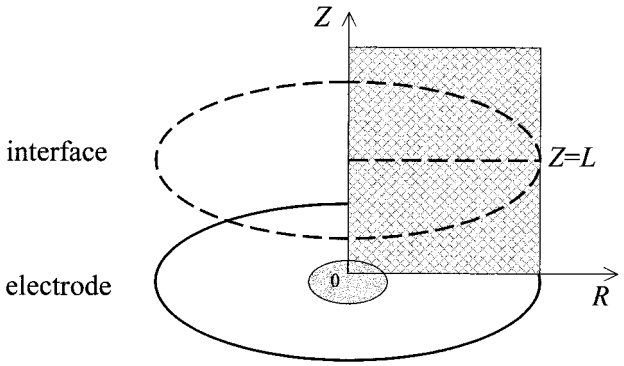

Figure 3. Schematic of the region (cross-hatched) represented by the concentration profiles in Figures 4 to 6. The ITIES is located at $Z = L$.

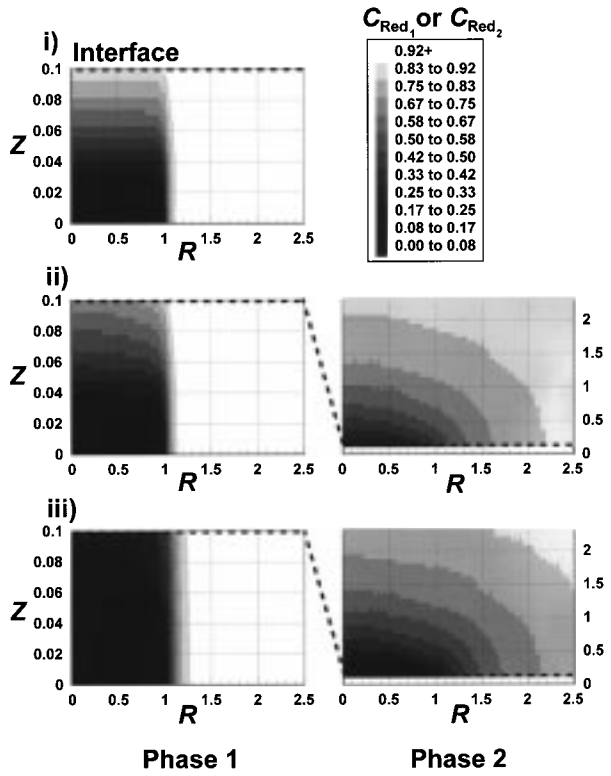

Figure 4. Steady-state concentration profiles for species Red_1 and Red_2 in phases 1 and 2, respectively, for $K = 100$ and $\gamma = 1$, with K_r taking the values (i) 1000, (ii) 10, and (iii) 5.

$K_r = 10$, and consequently a quasihemispherical diffusion field of Red_2 is established in phase 2 [Figure 4(ii)]. The effect is to diminish the extent of positive feedback, as reflected by the change in the phase 1 profile between Figure 4(i) and 4(ii) and evident by the lower current observed at close tip/interface separations, compared to the constant composition case [Figure 2(i)]. For $K_r = 5$, the depletion of Red_2 in phase 2 becomes very significant, such that the Red_1 profile in phase 1 has a considerable hindered diffusion component [Figure 4(iii)]. Although the tendency for depletion in phase 2 becomes less significant as the interfacial rate constant is decreased, there are still considerable diffusional limitations from Red_2 in phase 2 for $K = 10$, with $K_r = 10$ and 5 [Figure 5(ii) and (iii)]. Even for $K = 1$, Red_2 is depleted at the interface when $K_r = 10$ and 5 [Figure 6(ii) and (iii)].

The precise conditions under which the constant composition model is valid can be identified by plotting the calculated normalized current ratio derived from the full model, outlined herein, as a function of log K_r for a range of rate constants typically encountered in SECM feedback studies of ITIES. The results of this exercise are shown in Figure 7 for $\gamma = 1$, log-$(d/a) = -0.5$, -0.8, and -1.0, and K values from 2 to 1000. At low K_r (log $K_r = -2$), the concentration of Red_2 in phase 2

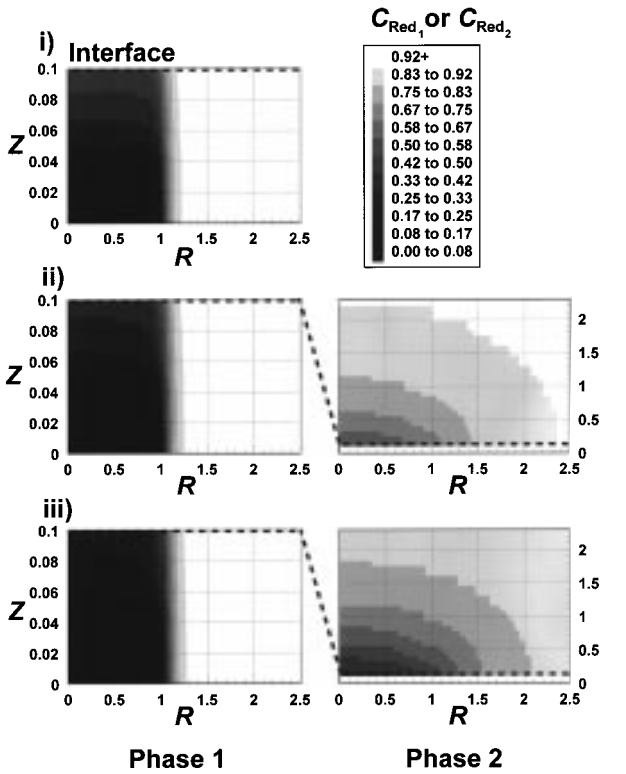

Figure 5. Steady-state concentration profiles for species Red_1 and Red_2 in phases 1 and 2, respectively, for $K = 10$ and $\gamma = 1$, with K_r taking the values (i) 1000, (ii) 10, and (iii) 5.

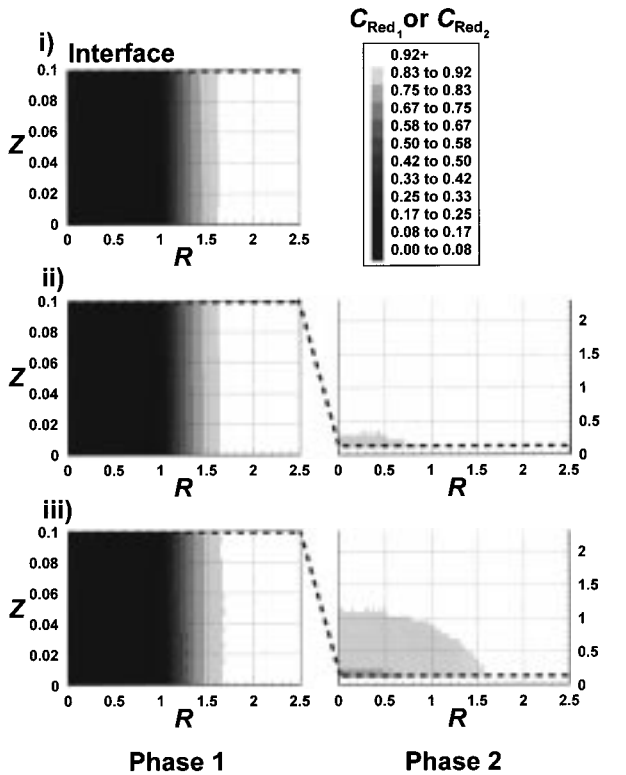

Figure 6. Steady-state concentration profiles for species Red_1 and Red_2 in phases 1 and 2, respectively, for $K = 1$ and $\gamma = 1$, with K_r taking the values (i) 1000, (ii) 10, and (iii) 5.

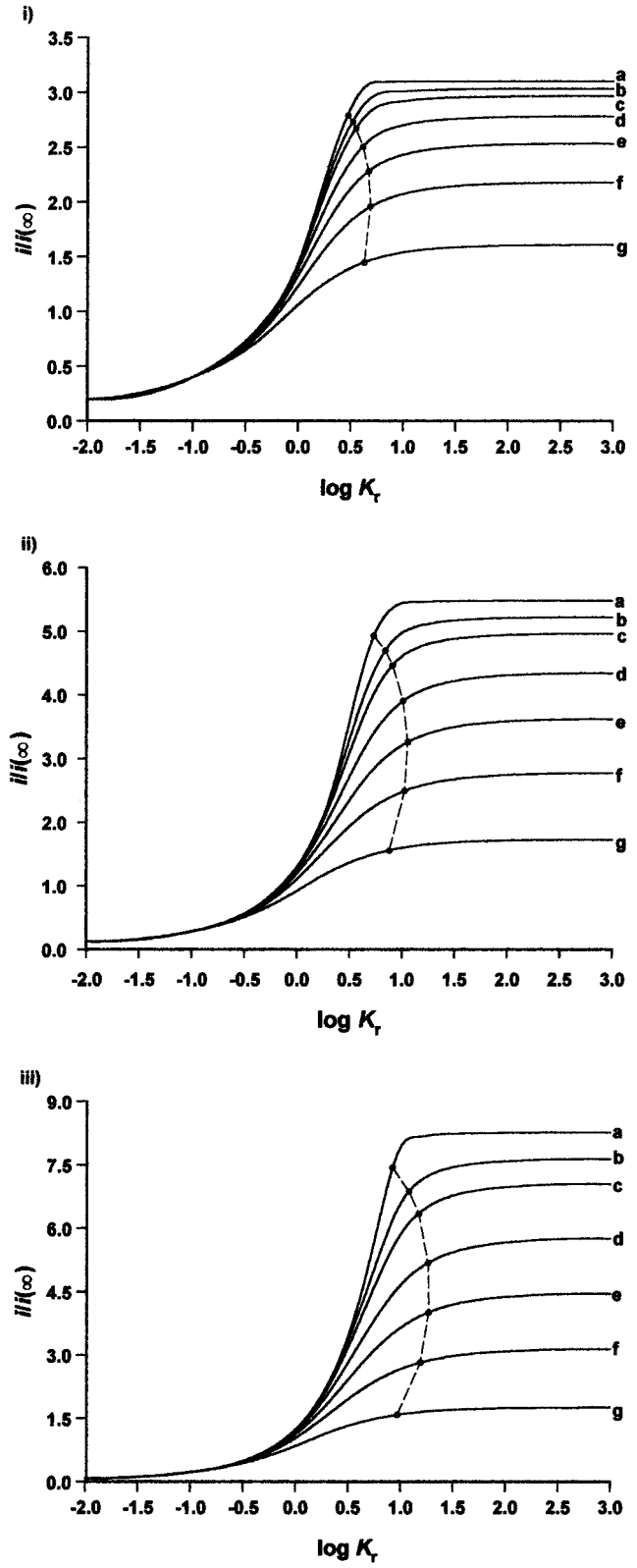

Figure 7. Working curves of normalized tip current versus log K_r for $\gamma = 1$, with K taking the values (a) 1000, (b) 100, (c) 50, (d) 20, (e) 10, (f) 5 and (g) 2. The data are for (i) $\log(d/a) = -0.5$, (ii) $\log(d/a) = -0.8$, (iii) $\log(d/a) = -1.0$. The region to the left of the dashed line is where the constant composition model tends to be invalid.

is so low that effectively negative feedback is observed at each separation considered (irrespective of the value of K). As K_r is increased the current ratio is enhanced to a K-dependent limiting value which holds when diffusional effects in phase 2 are

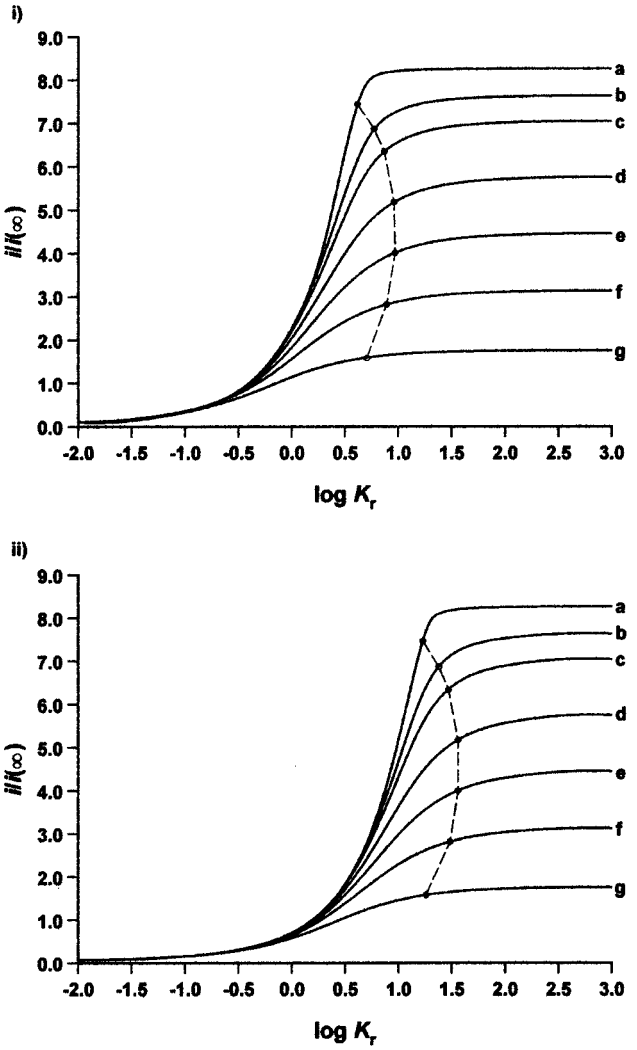

Figure 8. Working curves of normalized tip current versus log K_r for (i) $\gamma = 2$ and (ii) $\gamma = 0.5$, with $\log(d/a) = -1.0$. K takes the values (a) 1000, (b) 100, (c) 50, (d) 20, (e) 10, (f) 5, and (g) 2. The region to the left of the dashed line is where the constant composition model tends to be invalid.

negligible (generally $\log K_r > 2$). Between these two limits, the current ratio is sensitive to the value of K_r.

If we consider that an experimental measurement of $i/i(\infty)$, under arbitrary conditions of K_r, can be distinguished from the corresponding constant composition value, provided the former is at most 90% of the latter (which should generally be possible), the data in Figure 7 can be divided into zones to indicate the conditions under which the constant composition model tends to be valid and invalid. The dashed lines bisecting the working curves in Figure 7 indicate the borders between these two domains for different distances between the tip and the ITIES. As expected, the boundary shifts to higher K_r as d/a decreases, as a result of the higher mass transport rates promoted at close tip/interface separations. The boundaries also show a slight dependence on K, but, at the smallest d/a, the constant composition model is generally not a good approximation when $K_r < 10$ for all kinetic cases considered.

The constant composition approximation is both K_r- and γ-dependent. When the diffusion coefficient of Red_2 is greater than that of Red_1, the constant composition model is valid to lower K_r, as indicated by the data in Figure 8(i), simulated for $\gamma = 2$. Conversely, if Red_2 is characterized by a low diffusion coefficient compared to Red_1, the approximation breaks down at higher K_r, as illustrated in Figure 8(ii) for $\gamma = 0.5$.

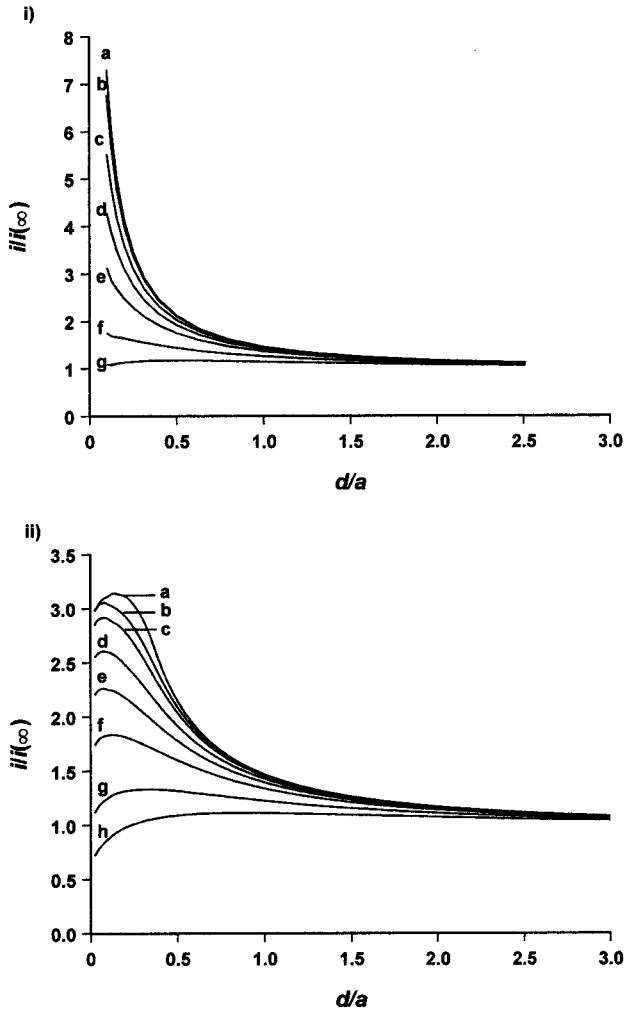

Figure 9. Simulated approach curves of $i/i(\infty)$ versus normalized tip/interface separation, d/a, for (i) constant composition conditions with K = (a) 100, (b) 50, (c) 20, (d) 10, (e) 5, (f) 2, and (g) 1; (ii) full model conditions with $K_r = 3$ and K = (a) 1000, (b) 100, (c) 50, (d) 20, (e) 10, (f) 5, (g) 2, and (h) 1.

In addition to extending the range of conditions under which SECM feedback measurements can be made at liquid/liquid interfaces, lifting the restriction on the composition of phase 2 is particularly beneficial for enhancing both the range and precision with which fast kinetics can be investigated. This is not only due to the fact that decreasing the bulk concentration of Red_2 in phase 2 lowers the dimensionless rate constant for the system (eq 17) but also because the approach curves in the fast kinetic limit are more readily distinguished from one another when $K_r < 10$. This point is well illustrated by the data presented in Figure 9, which shows simulated tip approach curves for a range of normalized rate constants (i) under the constant composition approximation and (ii) with $K_r = 3$ and $\gamma = 1$.

Although there are differences in the approach curves with the constant composition model, it would be extremely difficult to distinguish between any of the K cases practically, unless K was below 10. Even for $K = 10$, an uncertainty in the tip position from the interface of $\pm$ 0.1d/a would not allow the experimental behavior for this rate constant to be distinguished from the diffusion-controlled case. For a typical value of $D_{Red_1} = 10^{-5}$ cm^2 s^{-1} and electrode radius $a = 12.5$ μm, this corresponds to an effective first-order heterogeneous rate constant of just 0.08 cm s^{-1}. Assuming one needs $K_r \geq 20$ to ensure constant composition conditions and at least 0.5 mM of mediator in phase 1 for reasonable measurements (as in all previous experimental investigations of ITIES by SECM),[1,4,7] this corresponds to an upper limit on k_{12} of 8 cm s^{-1} M^{-1}. In contrast, for $K_r = 3$, the approach curves are such that ready kinetic discrimination should be possible for $K \leq 100$ [Figure 9(ii)]. For the same values of D_{Red_1} and a, with a bulk concentration of Red_2 in phase 2, $c^*_{Red_2} = 1.5$ mM, this corresponds to a bimolecular rate constant, k_{12}, of ca. 500 cm s^{-1} M^{-1}. It is also interesting to note that since the approach curves in Figure 9(ii) have peaks (at least for the fast kinetic cases that are most of interest), it is not actually necessary to know the tip to ITIES separation absolutely. Rather, the rate constant for the process of interest could be deduced simply by measuring the peak current value of a tip approach curve.

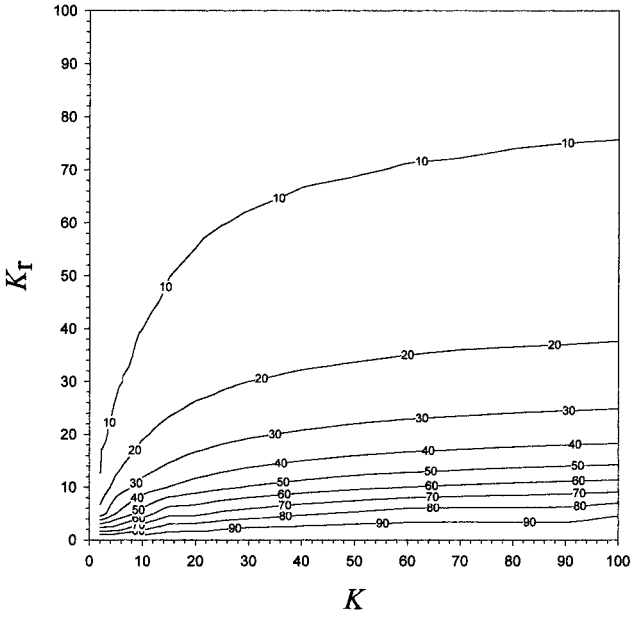

Figure 10. Contour plot of percentage error in the rate constant k_{12} that results from analyzing data in terms of the constant composition model, rather than the full model presented in this paper. The data are for a tip/ITIES separation, $d/a = 0.1$, with a range of K and K_r values.

A final assessment of the applicability of the constant composition assumption, compared to the full model, is shown in Figure 10. This is a plot of the percentage error in the interfacial rate constant that would result from analyzing experimental data at $\log(d/a) = -1.0$, obtained with arbitrary K_r, using the earlier constant composition theory.[1,19(b)] To use the constant composition model to analyze data obtained under conditions of finite K_r is to underestimate the rate constant; therefore, the errors in Figure 10 are the relative percentage underestimates of the rate constant. It can be seen that for $K_r > 40$, the constant composition model is a good one, resulting in errors of less than 10−15% over the full range of rate constants. For $K_r < 20$, however, sizeable errors result, particularly in the fast kinetic regime. This diagram can be used as a guide as to the likely errors involved in analyzing data for particular conditions with the constant composition model.

Experimental

Chemicals. $Na_4Fe(CN)_6$ from Johnson Matthey (Ward Hill, MA), Na_2EDTA, $FeCl_2 \cdot 4H_2O$, ZnPor, and benzonitrile from Aldrich (Milwaukee, WI), and benzene from Fluka Chemika (Switzerland) were used as received. Tetrahexylammonium perchlorate ($THAClO_4$; Fluka Chemika) was recrystallized twice from an ethyl acetate/ether (9:1) mixture and dried under vacuum overnight at room temperature. Tetrabutylammonium

tetrafluoroborate ($TBABF_4$; Southwestern Analytical Chemicals, Austin, TX) was recrystallized from acetone/ether. $Na_4Ru(CN)_6$ and $Na_4Mo(CN)_8$ were synthesized as reported previously.[7] Aqueous solutions with varying concentrations of reductants were generally prepared with 0.1 M NaCl and 0.1 M $NaClO_4$ as supporting electrolytes (for exceptions, see below). Aqueous solutions of $FeEDTA^{2-}$ were prepared by adding a stoichiometric amount of $FeCl_2 \cdot 4H_2O$ to deaerated solutions of Na_2-EDTA buffered with 0.01 M citrate at pH 4.8. Benzonitrile solutions, containing 0.25 M $THAClO_4$ and 0.3−1 mM ZnPor, were mixed with at least twice their volume of water by vigorous shaking and centrifuged to separate the organic solution from the aqueous phase. This procedure was repeated three to five times to remove trace amounts of surfactants from the organic phase that might adsorb on the benzonitrile/water interface. For experiments with $Na_4Fe(CN)_6$, benzene was used instead of benzonitrile. For experiments with $Na_4Ru(CN)_6$, 0.2 M $NaBF_4$ and 0.2 M $TBABF_4$ were used instead of 0.1 M $NaClO_4$ and 0.25 M $THAClO_4$, respectively. All aqueous solutions were prepared from deionized water (Milli-Q, Millipore Corp).

Electrodes and Electrochemical Cells. SECM tips were prepared by heat-sealing Pt wires (25-μm diameter, Goodfellow, Cambridge, U.K.) in glass capillaries as described previously.[21] The tip electrode was rinsed with ethanol and water and then polished and dried before each measurement. A three-electrode configuration (tip, auxiliary, and reference) was used in all experiments, and all electrodes were placed in the top (organic) phase. The SECM cell was described previously.[4] An ionic bridge containing 0.1 M NaCl and 0.1 M $NaClO_4$ was placed between the SCE reference electrode and organic solution, except for experiments with $Na_4Ru(CN)_6$, for which a Ag/AgCl wire was used as a reference electrode. Experiments with $FeEDTA^{2-}$ were carried out in a glovebag (Aldrich) under nitrogen.

SECM Apparatus and Procedure. A home-built SECM instrument[22] was employed for experiments with $Na_4Fe(CN)_6$, while a commercially available SECM (model CHI-900; CH Instruments, Cordova, TN) was used for measurements on other systems. In all SECM experiments, the tip electrode was biased at a potential corresponding to the plateau current of the oxidation wave of ZnPor to $ZnPor^{+\bullet}$. Approach curves were obtained by moving the tip toward the ITIES and recording the tip current, i, as a function of the distance, d.

Measurement of the Driving Force for Interfacial ET. For quantitative comparison of the ET rate constant, k_{12}, obtained for the different redox species, the driving force for the interfacial ET was measured as reported previously.[7] The formal potentials for most of the aqueous redox species and ZnPor in benzene were evaluated as the half-wave potential, $E_{1/2}$, of the nernstian steady-state voltammograms. The formal potential for the $FeEDTA^{2-}$ was found from the quasireversible steady-state voltammogram, using a procedure reported previously.[23] These voltammograms were measured with respect to the SCE reference electrode with the same ionic bridge as used for SECM measurements. The difference of half-wave potentials for an aqueous redox species and ZnPor is

$$\Delta E_{1/2} = \Delta E^\circ + \Delta\phi \qquad (23)$$

where ΔE° is the difference of formal potentials of the aqueous redox species and ZnPor, and $\Delta\phi$ is the relative value of the potential drop across the ITIES. $\Delta E_{1/2}$ gives the absolute value of the driving force according to eqs 5 and 7 in ref 7.

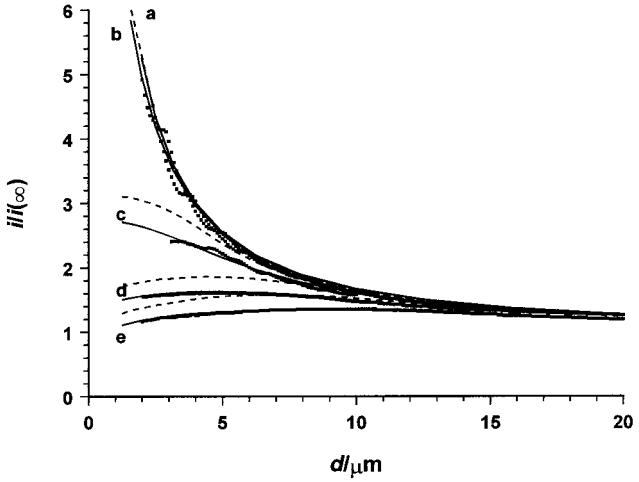

Figure 11. Experimental approach curves (■) for the oxidation of ZnPor at a tip UME in benzene approaching a benzene/aqueous interface, with the aqueous phase containing $Fe(CN)_6^{4-}$. The bulk concentration conditions in the organic and aqueous phases, respectively, were as follows: (a) [ZnPor]* = 0.500 mM, $[Fe(CN)_6^{4-}]^*$ = 7.00 mM; (b) [ZnPor]* = 0.500 mM, $[Fe(CN)_6^{4-}]^*$ = 3.50 mM; (c) [ZnPor]* = 0.380 mM, $[Fe(CN)_6^{4-}]^*$ = 0.700 mM; (d) [ZnPor]* = 0.380 mM, $[Fe(CN)_6^{4-}]^*$ = 0.350 mM; (e) [ZnPor]* = 0.380 mM, $[Fe(CN)_6^{4-}]^*$ = 0.255 mM. The solid lines show the behavior predicted for $\gamma = 1.7$ and a bimolecular rate constant, $k_{12} = 91$ cm s^{-1} M^{-1}, while the dashed lines show the behavior for a diffusion-controlled process for each of the five cases considered, simulated using the model described herein. The diffusion-controlled characteristics for the two cases with the highest K_r are indistinguishable.

Experimental Results and Discussion

A set of steady-state approach curves of $i/i(\infty)$ versus tip/interface separation, d, is shown in Figure 11 for the oxidation of ZnPor to $ZnPor^{+\bullet}$, in a benzene phase, at an UME tip translated toward the interface with an aqueous solution, containing various concentrations of $Fe(CN)_6^{4-}$. This is a useful system to begin the assessment of the new model, since the driving force for the reaction is large, with a measured $\Delta E_{1/2}$ of 585 mV. Previous SECM investigations of the kinetics of this process, under constant composition conditions, found only that the rate constant was too high to be measured, with the process deduced to be diffusion-controlled, i.e., showing an approach curve indistinguishable from that characteristic of total positive feedback.[7]

The experimental data in Figure 11 are shown alongside the best fits to the model presented herein. These simulations were carried out for $\gamma = 1.7$, given the measured values of $D_{ZnPor} = 4.0 \times 10^{-6}$ cm^2 s^{-1} and $D_{Fe(CN)_6^{4-}} = 6.7 \times 10^{-6}$ cm^2 s^{-1} in the two solvents of interest. For the highest two concentration ratios considered (K_r = 14 and 7), the interfacial redox reaction appears to be diffusion controlled and the rate constant cannot be determined. However, as the value of K_r is decreased, by employing smaller concentrations of $Fe(CN)_6^{4-}$ in the aqueous phase, it becomes possible to distinguish the measured behavior from the predictions of the diffusion-controlled cases. For the lowest three K_r values investigated, the experimental current−distance data lie below the simulated characteristics for a diffusion-controlled process and can be analyzed well in terms of a unique rate constant, $k_{12} = 91$ cm s^{-1} M^{-1}.

In addition to expanding the range of rate constants that can be studied, lifting the constant composition restriction on phase 2 also enhances the precision and certainty with which rate measurements can be made. As outlined in the theoretical results and discussion section, the measurement of rapid rate constants,

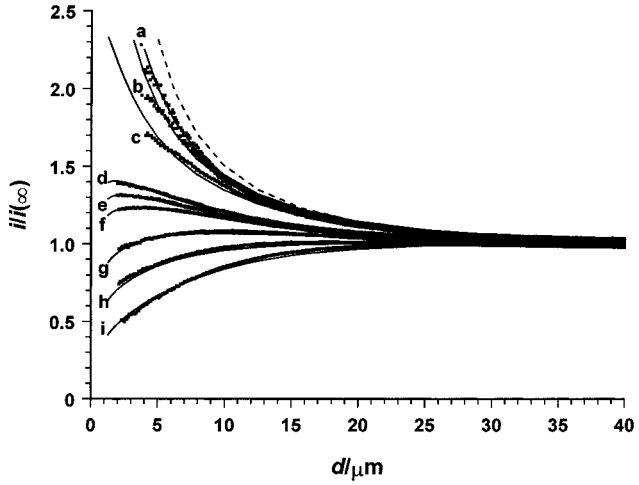

Figure 12. Experimental approach curves (■) for the oxidation of ZnPor at a tip UME in benzonitrile approaching a benzonitrile/aqueous interface, with the aqueous phase containing $Mo(CN)_8^{4-}$. For all experiments, ZnPor was present at a concentration of 0.500 mM, while the concentration of $Mo(CN)_8^{4-}$ was such that the following values of K_r resulted: (a) 14, (b) 10, (c) 6, (d) 4, (e) 3, (f) 2, (g) 1.2, (h) 0.8, and (i) 0.4. The solid lines are the best fits of the experimental data to theory for $\gamma = 3.2$ with k_{12}/cm s^{-1} M^{-1} = (a) 2.75, (b) 2.75, (c) 2.75, (d) 1.75, (e) 2.1, (f) 3.0, (g) 3.5, (h) 3.25, and (i) 3.0. The dashed line shows the predicted behavior for a diffusion-controlled process under constant composition conditions.

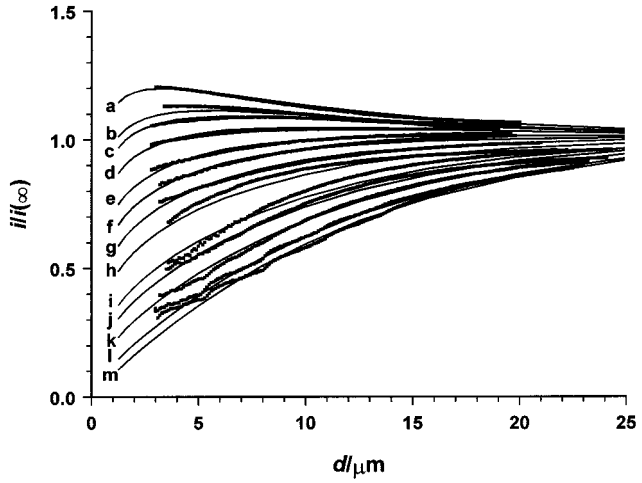

Figure 13. Experimental approach curves (■) for the oxidation of ZnPor at a tip UME in benzonitrile approaching a benzonitrile/aqueous interface, with the aqueous phase containing $Ru(CN)_6^{4-}$. For all experiments, ZnPor was present at a concentration of 1.00 mM, while the concentration of $Ru(CN)_6^{4-}$ was such that the following values of K_r resulted: (a) 9.8, (b) 8.2, (c) 7.7, (d) 6.6, (e) 5.3, (f) 4.5, (g) 3.7, (h) 2.8, (i) 1.7, (j) 1.3, (k) 0.8, (l) 0.3, and (m) 0.1. The solid lines are the best fits of the experimental data to theory with $k_{12} = 0.25$ cm s^{-1} M^{-1} and $\gamma = 2.8$.

under constant composition conditions, requires that similar approach curves involving enhanced currents at close distances can be distinguished from one another, placing considerable importance on the accurate and reproducible attainment of close tip/interface separations. In contrast, by working under conditions of lower K_r the approach curves flatten and indeed may peak as the tip/interface separation is decreased from high to low values. In the latter situation, uncertainties in the separation between the tip and the interface become less important, as the magnitude of the peak current alone is the unequivocal pointer to the kinetics of the interfacial process. This effect is found in practice in the two approach curves with the lowest K_r in Figure 11.

The key points introduced above with $Fe(CN)_6^{4-}$ as the reductant are further emphasized in Figure 12, which shows an extensive set of approach curves obtained with $Mo(CN)_8^{4-}$ as the reductant in the aqueous phase. These measurements were made with benzonitrile, rather than benzene, as the organic solvent. The experimental data can be analyzed very well in terms of a value of k_{12} of 2.5 ± 0.75 cm s^{-1} M^{-1}, given $\gamma = 3.2$, based on measured diffusion coefficients for ZnPor and $Mo(CN)_8^{4-}$, respectively, of 2.4×10^{-6} cm^2 s^{-1} and 7.2×10^{-6} cm^2 s^{-1} in the two solvents of interest. However, it can be seen again that even with this relatively low rate constant, tip/interface separations have to be known with high precision to make a kinetic assignment of the data obtained under conditions where constant composition of the second phase can be assumed (case a, with $K_r = 14$). In contrast, by lifting the restriction on the composition of phase 2, an assignment of k_{12} is readily achieved.

Although it is difficult to make a precise comparison of the rate constants obtained from the data in Figures 11 and 12, because of the different organic solvents used, the decrease in rate constant between $Fe(CN)_6^{4-}$ and $Mo(CN)_8^{4-}$ is at least, in part, due to a lower driving force in the latter case, with $\Delta E_{1/2} = 140$ mV. As the driving force is reduced further, the rate constant decreases, as evidenced by the data in Figure 13, for experiments with $Ru(CN)_6^{4-}$ as the reductant in the aqueous phase, with ZnPor again the initial species in benzonitrile. In this case, $\Delta E_{1/2} = 70$ mV and the rate constant $k_{12} = 0.25$ cm s^{-1} M^{-1}. For this system, it is particularly satisfying that there is an excellent fit of the data to the new model over 2 orders of magnitude in K_r, from a value of 9.8 down to 0.1. In analyzing these data, a value of $\gamma = 2.8$ was used, based on the measured diffusion coefficient of $Ru(CN)_6^{4-}$ in the aqueous phase of 6.7×10^{-6} cm^2 s^{-1}.

As a final example, a system was investigated where the driving force was larger than that of the $Fe(CN)_6^{4-}$ case considered in Figure 11. Using $FeEDTA^{2-}$ as the reductant in the aqueous phase, with ZnPor again oxidized at the tip in benzonitrile solution, a driving force, $\Delta E_{1/2} = 776$ mV, was established. Steady-state current distance approach curves for this system are shown in Figure 14 for K_r over the range 2.4 to 8.2. A value of $\gamma = 2.4$ was employed to fit the experimental data to theory, on the basis of the measured diffusion coefficient for $FeEDTA^{2-}$ in the aqueous phase of 5.7×10^{-6} cm^2 s^{-1}. The data can be analyzed in terms of a fairly consistent value of k_{12} in the range 7.5−10 cm s^{-1} M^{-1}. These data show clearly again that it becomes increasingly easier to identify an accurate value of k_{12}, distinct from the diffusion-controlled behavior, by decreasing the K_r value.

The rate constant derived from the data in Figure 14, with $FeEDTA^{2-}$ is lower than with $Fe(CN)_6^{4-}$ as the reductant, even though the driving force, based on $\Delta E_{1/2}$, is apparently higher in the former case. Although this paper is concerned with a new general model for SECM feedback at ITIES with a focus on the role of diffusion of the redox-active species in phase 2, some comment on the rate constants derived in the four systems is warranted. A plot of log k_{12} vs driving force is shown in Figure 15. Although the solvent used for the $Fe(CN)_6^{4-}$ study was different than that of the other three reductants, the overall trend is consistent with the predictions of Marcus theory,[24] showing first an increase in the reaction rate with increased driving force, followed by a decrease in the inverted region. The Marcus λ values probably differ for the various couples, but a general plot according to Marcus theory with $\lambda = 0.55$ eV (and an arbitrary maximum rate constant of about 50 cm s^{-1} M^{-1}) shows a trend consistent with the data. While more detailed studies with more couples are needed to confirm these

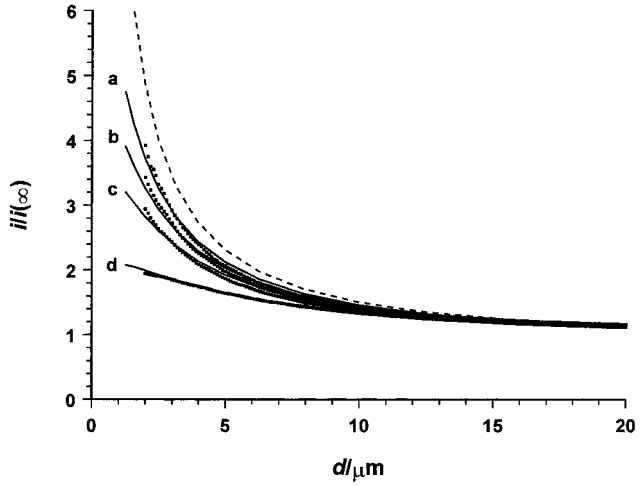

Figure 14. Experimental approach curves (■) for the oxidation of ZnPor at a tip UME in benzonitrile approaching a benzonitrile/aqueous interface, with the aqueous phase containing $FeEDTA^{2-}$. For all experiments, ZnPor was present at a concentration of 0.500 mM, while the concentration of $FeEDTA^{2-}$ was such that the following values of K_r resulted: (a) 9.8, (b) 5.4, (c) 3.8, and (d) 2.4. The solid lines are the best fits of the experimental data to theory with $\gamma = 2.4$ and k_{12}/cm s^{-1} M^{-1} values of (a−c) 10 and (d) 7.5. The dashed line shows the predicted behavior for a diffusion-controlled process under constant composition conditions.

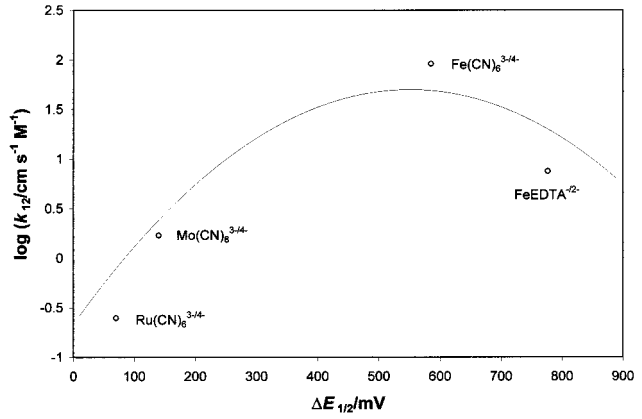

Figure 15. Plot of log k_{12} versus $\Delta E_{1/2}$ derived from the data for the four systems in Figures 11−14. The solid line is expected behavior based on Marcus theory for $\lambda = 0.55$ eV and a maximum rate constant of 50 cm s^{-1} M^{-1}.

results, the proposed existence of interfacial inverted region behavior suggested by these studies is consistent with a previous study of the electron transfer at an ITIES modified with a monolayer of surfactant.[7] The methodology outlined in this paper should be useful in enhancing the range of kinetics open to quantitative investigation at the ITIES by the SECM technique.

Conclusions

By developing a full treatment for SECM feedback for the case of a redox reaction at an ITIES, a fuller range of reaction conditions may now be explored than could with earlier limiting models based on the constant composition approximation. The conditions under which the latter approximation is valid have been identified. For a given tip/substrate separation and tip geometry, the key parameters are the relative diffusion coefficients and concentrations of the redox reactants in the two phases. When the diffusion coefficients of the redox-active species in the two phases are similar, it is recommended that the concentration of the redox couple in the second phase be 15 to 20 times that in the phase containing the probe, if the constant composition theory is to be used.

Lifting the restriction on the composition of the second phase to allow the use of a relatively low concentration of redox-active mediator has been shown to result in considerable advantages for the study of rapid kinetics. In particular, rate processes can be characterized that would appear purely diffusion-controlled under constant composition conditions. Thus, it has been possible to measure the kinetics of the reaction between $ZnPor^{+\bullet}$ and $Fe(CN)_6^{4-}$, which has appeared diffusion-controlled in previous SECM studies.

The rate constants obtained for the four systems investigated generally follow a trend with driving force consistent with Marcus theory, in particular suggesting inverted region behavior for interfacial electron transfer. Further studies of ET at ITIES are underway using the methodology and theory outlined in this paper.

Acknowledgment. The support of this research by the EPSRC (P.R.U. and A.L.B.), the National Science Foundation (CHE9870762), and the Robert A. Welch Foundation (A.J.B.) is gratefully acknowledged. S.A. expresses thanks for a post-doctoral fellowship from the Japan Society for the Promotion of Science.

References and Notes

(1) Wei, C.; Bard, A. J.; Mirkin, M. V. *J. Phys. Chem.* **1995**, *99*, 16033.
(2) Solomon, T,; Bard, A. J. *J. Phys. Chem.* **1995**, *99*, 17487.
(3) Selzer, Y.; Mandler, D. *J. Electroanal. Chem.* **1996**, *409*, 15.
(4) Tsionsky, M.; Bard, A. J.; Mirkin, M. V. *J. Phys. Chem.* **1996**, *100*, 17881.
(5) Shao, Y.; Mirkin, M. V.; Rusling, J. F. *J. Phys. Chem. B* **1997**, *101*, 3202.
(6) Delville, M.-H.; Tsionsky, M.; Bard, A. J. *Langmuir* **1998**, *14*, 2774.
(7) Tsionsky, M.; Bard, A. J.; Mirkin, M. V. *J. Am. Chem. Soc.* **1997**, *119*, 10785.
(8) Shao, Y.; Mirkin, M. V. *J. Electroanal. Chem.* **1997**, *439*, 137.
(9) Slevin, C. J.; Umbers, J. A.; Atherton, J. H.; Unwin, P. R. *J. Chem. Soc., Faraday Trans.* **1996**, *92*, 5177.
(10) Barker, A. L.; Macpherson, J. V.; Slevin, C. J.; Unwin, P. R. *J. Phys. Chem. B* **1998**, *102*, 1586.
(11) Shao, Y.; Mirkin, M. V. *J. Phys. Chem. B* **1998**, *102*, 9915.
(12) Slevin, C. J.; Macpherson, J. V.; Unwin, P. R. *J. Phys. Chem. B* **1997**, *101*, 10851.
(13) Bard, A. J.; Fan, F.-R. F.; Mirkin, M. V. In *Electroanalytical Chemistry*; Bard, A. J., Ed.; Marcel Dekker: New York, 1994; Vol. 18, p 243.
(14) Martin, R. D.; Unwin, P. R. *J. Electroanal. Chem.* **1997**, *439*, 123.
(15) Kwak, J.; Bard, A. J. *Anal. Chem.* **1989**, *61*, 1221.
(16) Macpherson, J. V.; Unwin, P. R. *J. Phys. Chem.* **1994**, *98*, 1704. (b) Macpherson, J. V.; Unwin, P. R. *J. Phys. Chem.* **1994**, *98*, 3109. (c) Macpherson, J. V.; Unwin, P. R. *J. Phys. Chem.* **1995**, *99*, 3338. (d) Macpherson, J. V.; Unwin, P. R. *J. Phys. Chem.* **1995**, *99*, 14824. (e) Macpherson, J. V.; Unwin, P. R. *J. Phys. Chem.* **1996**, *100*, 19475.
(17) Saito, Y. *Rev. Polarogr. Jpn.* **1968**, *15*, 177.
(18) Peaceman, D. W.; Rachford, H. H. *J. Soc. Ind. Appl. Math.* **1955**, *3*, 28.
(19) (a) Unwin, P. R.; Bard, A. J. *J. Phys. Chem.* **1991**, *95*, 7814. (b) Bard, A. J.; Mirkin, M. V.; Unwin, P. R.; Wipf, D. O. *J. Phys. Chem.* **1992**, *96*, 1861. (c) Pierce, D. T.; Unwin, P. R.; Bard, A. J. *Anal. Chem.* **1992**, *64*, 1795. (d) Unwin, P. R.; Bard, A. J. *J. Phys. Chem.* **1992**, *96*, 5035.
(20) (a) Lapidus, L.; Pinder, G. F. *Numerical Solutions of Partial Differential Equations in Science and Engineering*; Wiley: New York, 1982. (b) Ames, W. F. *Numerical Methods of Partial Differential Equations*; Wiley: New York, 1977.
(21) Bard, A. J.; Fan, F.-R. F.; Kwak, J.; Lev, O. *Anal. Chem.* **1989**, *61*, 1794.
(22) Wipf, D. O.; Bard, A. J. *J. Electrochem. Soc.* **1991**, *138*, 489.
(23) Mirkin, M. V.; Bard, A. J. *Anal. Chem.* **1992**, *64*, 2293.
(24) Marcus, R. A.; Sutin, N. *Biochim. Biophys. Acta* **1985**, *811*, 265.